HHS Public Access

Author manuscript

Bone. Author manuscript; available in PMC 2016 December 01.

Published in final edited form as:

Bone. 2015 December ; 81: 524–532. doi:10.1016/j.bone.2015.09.002.

Hedgehog signaling mediates woven bone formation and vascularization during stress fracture healing

Nikolas H. Kazmers, M.D., M.S.E.[1,*,a], **Jennifer A. McKenzie, Ph.D.**[1,a], **Tony S. Shen, B.A.**[1], **Fanxin Long, Ph.D.**[1,2,3], and **Matthew J. Silva, Ph.D.**[1,4]

[1]Department of Orthopaedic Surgery, Washington University, St. Louis, MO, USA, Campus Box 8233, 660 South Euclid Avenue, St. Louis, MO 63110, USA

[2]Department of Medicine, Washington University, St. Louis, MO, USA

[3]Department of Developmental Biology, Washington University, St. Louis, MO, USA

[4]Department of Biomedical Engineering, Washington University, St. Louis, MO, USA

Abstract

Hedgehog (Hh) signaling is critical in developmental osteogenesis, and recent studies suggest it may also play a role in regulating osteogenic gene expression in the post-natal setting. However, there is a void of studies directly assessing the effect of Hh inhibition on post-natal osteogenesis. This study utilized a cyclic loading-induced ulnar stress fracture model to evaluate the hypothesis that Hh signaling contributes to osteogenesis and angiogenesis during stress fracture healing. Immediately prior to loading, adult rats were given GDC-0449 (Vismodegib - a selective Hh pathway inhibitor; 50mg/kg orally twice daily), or vehicle. Hh signaling was upregulated in response to stress fracture at 3d (Ptch1, Gli1 expression), and was markedly inhibited by GDC-0449 at 1d and 3d in the loaded and non-loaded ulnae. GDC-0449 did not affect Hh ligand expression (Shh, Ihh, Dhh) at 1d, but decreased Shh expression by 37% at 3d. GDC-0449 decreased woven bone volume (−37%) and mineral density (−17%) at 7d. Dynamic histomorphometry revealed that the 7d callus was composed predominantly of woven bone in both groups. The observed reduction in woven bone occurred concomitantly with decreased expression of Alpl and Ibsp, but was not associated with differences in early cellular proliferation (as determined by callus PCNA staining at 3d), osteoblastic differentiation (Osx expression at 1d and 3d), chondrogenic gene expression (Acan, Sox9, and Col2α1 expression at 1d and 3d), or bone resorption metrics (callus TRAP staining at 3d, Rankl and Opg expression at 1d and 3d). To

[*]Corresponding author: nkazmers@gmail.com.

[a]NHK and JAM contributed equally to this study.

Disclosures:

None

Authors' Roles:

Study design: NHK, JAM, FL, and MJS. Study conduct: NHK, JAM, TS, and FL. Data collection: NHK, JAM, and TS. Data analysis: NHK and JAM. Data interpretation: NHK, JAM, FL, MJS. Drafting manuscript: NHK. Revising manuscript content: NHK, JAM, and MJS. Approving final version of manuscript: NHK, JAM, TS, FL, MJS. NHK, JAM, and MJS take responsibility for the integrity of the data analysis.

evaluate angiogenesis, vWF immunohistochemistry showed that GDC-0449 reduced fracture callus blood vessel density by 55% at 3d, which was associated with increased Hif1α gene expression (+30%). Dynamic histomorphometric analysis demonstrated that GDC-0449 also inhibited lamellar bone formation. Lamellar bone analysis of the loaded limb (directly adjacent to the woven bone callus) showed that GDC-0449 significantly decreased mineral apposition rate (MAR) and bone formation rate (BFR/BS) (−17% and −20%, respectively). Lamellar BFR/BS in the non-loaded ulna was also significantly decreased (−37%), indicating that Hh signaling was required for normal bone modeling. In conclusion, Hh signaling plays an important role in post-natal osteogenesis in the setting of stress fracture healing, mediating its effects directly through regulation of bone formation and angiogenesis.

Keywords

Hedgehog; woven bone; fracture healing; osteogenesis; angiogenesis

Introduction

Multiple clinically relevant scenarios spanning virtually all orthopedic subspecialties involve osteogenesis, including spinal fusion, distraction osteogenesis, physiologic anabolism secondary to load-bearing exercises, and fracture healing. The sheer number of orthopedic patients affected by conditions requiring bone healing, the associated treatment and recovery process, and potential complications, all place a significant burden on society in terms of patient morbidity and loss of productivity. Therefore, further elucidation of the pathways mediating osteogenesis in the adult skeleton may provide an opportunity to develop novel therapeutic strategies that enhance bone healing or prevent skeletal fragility.

Hedgehog (Hh) proteins are fundamental to animal development and are conserved in species ranging from *Drosophila melanogaster* to humans [1, 2]. The mammalian family of Hh proteins includes Sonic hedgehog (Shh), Desert hedgehog (Dhh), and Indian hedgehog (Ihh). These ligands signal through a mechanism involving two transmembrane proteins: Patched homolog 1 (Ptch1) and Smoothened (Smo) [3]. Hh binding to Ptch1 on the cell surface relieves the inhibition of Smo and activates an intracellular signaling cascade, resulting in increased transcription of downstream genes including glioma-associated oncogene-1 (Gli1) [4, 5], Hedgehog-interacting protein-1 (Hip1) [6], and Ptch1 itself. Thus, Ptch1 is a negative regulator of Hh signaling through this negative feedback loop, and increased Ptch1 expression is a marker of increased Hh pathway activation [7, 8]. Exogenous modulators of the pathway include Hh inhibitor GDC-0449 (Vismodegib) that acts directly on Smo [8–10]. The mechanism of action, pharmacokinetics, and pharmacodynamics of GDC-0449 have been studied extensively, mostly in the setting of cancer [9–13].

The Hh pathway is known to play a critical regulatory role in the context of embryonic limb patterning [14–17] and osteogenesis [18–21]. Ihh is required for development of perichondrial osteoblasts and vascularization of endochondral bone [14, 21], indicating that

Hh signaling is key to the coupling of osteogenesis and angiogenesis during skeletal development.

The role of Hh signaling in post-natal osteogenesis is poorly understood especially in the context of bone healing. Upgregulated Hh signaling was observed during healing of murine rib fractures [22] and rat ulna stress fractures [23], and Ihh expression was seen with healing of fractures [24, 25]. However, it remains unclear whether these observations represent a causal mechanism, or merely correlation. A recent study not only confirmed increased expression of Hh pathway components after fracture (stabilized murine tibial fractures), but also showed that both ubiquitous and osteoblast-specific Hh activation increased fracture callus matrix deposition (%BV/TV) [26]. Osteoblast-specific Hh inhibition, but not ubiquitous inhibition, led to a statistically significant decrease in fracture callus volume as compared to controls [26]. However, the mechanism responsible for these findings is yet to be elucidated.

In combination, these studies [18, 19, 22–26] provide support for the role of Hh signaling in endochondral bone repair. Our goal was to extend these findings in two novel ways. First, we utilized the systemic Hh antagonist GDC-0449 to determine whether pharmacological manipulation of the pathway affected bone repair. Second, we assessed the role of Hh in stress fracture healing, which is predominantly a non-endochondral repair process. We hypothesized that the woven bone healing response to stress fracture is a Hh-dependent process. Additionally, we hypothesized that the angiogenic response to stress fracture is also Hh-dependent. In order to investigate these hypotheses, we used a previously-described fatigue loading protocol to create mid-diaphyseal stress fractures in adult rat ulnae [23, 27, 28]. The experimental group was treated with the Hh inhibitor GDC-0449 and compared to a vehicle group. Differences were examined using quantitative real-time PCR (qRT-PCR), microCT, immunohistochemistry and dynamic histomorphometry. Our results demonstrate that Hh signaling contributes to the osteognenic and angiogenic response during stress fracture healing.

Materials and Methods

Animals

A total of 70 male Fischer F344 rats (Harlan) were obtained at 13–14 weeks of age and housed until ready for mechanical loading at 18–22 weeks of age (340±30g). After mild sedation with isoflurane (1–3%), treatment group rats were administered an initial dose of GDC-0449 (50mg/kg; 50mg/ml solution in DMSO) immediately prior to mechanical loading that was continued twice daily by oral gavage until sacrifice. Using the identical dosing schedule, control group rats received an equivalent volume of DMSO vehicle (1ml/kg twice daily by oral gavage). Treatment and vehicle animals were housed separately. Access to chow and water was *ad libitum*, and cage activity was unrestricted. Rat weight was recorded daily. All protocols were approved by the Animal Studies Committee at Washington University in St. Louis.

Mechanical loading

Rats were anesthetized (1–3% isoflurane). Previously-described fatigue-loading methods were used to produce a right ulna (RU) mid-diaphyseal stress fracture (time point defined as 0d) [23, 28, 29]. To summarize, the right ulna olecranon process and flexed carpus were placed in custom fixtures of a servohydraulic materials testing system (Instron 8841). A 0.3 N compressive preload was applied, followed by an axial 18 N, 2 Hz haversine waveform until a peak displacement of 1.3 mm occurred relative to the 10^{th} cycle (equivalent to 65% of the average total displacement to full fracture). These loading parameters consistently produced a non-displaced, oblique fatigue/stress fracture on the concave (compression) surface of the ulna, which was followed by a woven bone healing response histologically similar to intramembranous fracture repair [28, 29]. Buprenorphine (0.05 mg/kg intramuscular) was provided for analgesia. The contralateral left ulna (LU) served as an internal non-loaded control. Rats were returned to their cages, recovered from anesthesia, and were able to ambulate without complications.

Gene expression

After mechanical loading, rats were euthanized with CO_2 asphyxiation at 1d or 3d (28 rats total; n=6–7/group/time point) for gene expression using qRT-PCR as previously described [23]. Bilateral ulnae were immediately dissected without disrupting the periosteum, and frozen in liquid nitrogen. Each ulna was processed individually. The central 5mm of each ulna (containing the stress fracture site and callus) was isolated and pulverized. Each sample was reconstituted in Trizol (Ambion). Chloroform was added, and the nucleic acid phase was isolated using phase lock gel tubes (Eppendorf). Total RNA was isolated using an RNeasy mini kit (Qiagen) and DNase I (Qiagen) was applied, as per manufacturer's instructions. RNA concentration was quantified (ND-1000, Nanodrop), and RNA integrity was evaluated (Bioanalyzer 2100, Agilent Technologies). Before proceeding, samples were required to meet quality standards including 260/280 nm absorbance ratios of 1.8–2.1 (Nanodrop) and electrophoretograms consistent with RNA integrity numbers (RIN) ≥7 (Bioanalyzer 2100). First strand cDNA was produced (iScript, Biorad) from 500ng of total RNA. qRT-PCR was conducted in triplicate with a reaction volume of 20μl using Power SYBR green detection (StepOnePlus™, Applied Biosystems). A total of 17 target genes were evaluated: three Hh pathway mediators - Gli1, Ptch1, and Hhip; three Hh ligands - Shh, Ihh, and Dhh; three osteogenic genes - alkaline phosphatase liver/bone/kidney [Alpl], osterix [Osx], and bone sialoprotein [Ibsp]; three chondrogenic genes – aggrecan [Acan], sex determining region Y – box 9 [Sox9], and collagen type 2-α1 [Col2α1]; two angiogenic genes - hypoxia-inducible factor 1 [Hif1α], and platelet/endothelial cell adhesion molecule-1 [Pecam1]; two osteoclastogenesis regulatory genes – receptor activator of nuclear factor κB ligand [Tnfsf11 (Rankl)], and osteoprotegerin [Tnfrsf11b (Opg)]; and one validated reference gene – pumilio homolog 1 [Pum1]. Primers were either previously validated (Bsp, Osx, Ptch1, Pecam1, Hif1a) [23, 29], or purchased as predesigned sets and validated prior to use (QuantiTect Primer Assays, Qiagen [Pum1:QT01607396, Gli1:QT01586662, Hhip:QT01566663, Ihh:QT01618113, Dhh:QT01593697] or PrimeTime qPCR primers, IDT [Shh:Rn.PT.53a.8183165, Sox9:Rn.PT.53a.29440750, Col2a1:Rn.PT.53a.13642555, Alpl:Rn.PT.53a.10731288, Acan:Rn.PT.53a.9306870], Tnfsf11: Rn.PT.58.9292526, Tnfrsf11b: Rn.PT.58.11476004). Relative quantification of gene expression was examined

after first normalizing to Pum1 ($2^{-\Delta Cq}$); in some cases expression was further examined after normalizing loaded RU relative to the non-loaded LU ($2^{-\Delta\Delta Cq}$).

Micro computed tomography (microCT)

Right forelimbs (n=13–14/group) underwent microCT imaging as previously described 7d after mechanical loading (mCT40, Scanco Medical; 55 kV, 200 ms, 16 μm resolution) [23, 27, 28]. The central 14 mm of each ulna containing the entire fracture callus was chosen as the region of interest. The manufacturer's software (μCT v6.0) was used to determine longitudinal crack extent by measuring the distance between the most proximal and most distal aspect of the fracture, woven bone volume (Σ(*periosteal bone area – cortical area*) * *slice thickness*), woven bone mineral density (BMD), and tissue mineral density (TMD) of the cortical bone.

Dynamic histomorphometry

Dynamic histomorphometric analysis was performed at 7d on plastic embedded cortical sections (loaded RU and non-loaded LU transverse sections, n=9–11) to assess bone formation at the site of stress fracture, which was our primary interest. Based on preliminary results showing an effect of GDC-0449 on woven and lamellar bone formation at these cortical sites, we analyzed cancellous sections (non-loaded tibia longitudinal sections, n=9–10) to assess bone formation at a remote site. In brief, calcein green (5mg/kg intraperitoneal, Sigma) was administered immediately following mechanical loading, and alizarin-complexone (30mg/kg intraperitoneal, Sigma) was given 5d after loading. Rats were euthanized with CO_2 asphyxiation at 7d, and ulnae were embedded in methylmethacrylate (Sigma) using standard procedures. Using microCT to locate woven bone, sections of 100μm thickness were cut transversely for both ulnae at the location of the callus midpoint and adjacent to the most proximal extent of the fracture callus (lamellar sections) (Leica Microsystems, SP 1600). Longitudinal (sagittal) cancellous sections were made at the center of the tibia. Each section was mounted on a glass slide, ground down to 35–50 μm thickness, and imaged on a fluorescent microscope (Olympus, DP-30) using fluorescein isothiocyanate and tetramethylrhodamineisothiocyanate filters for calcein and alizarin, respectively. Bioquant software was used for analysis of periosteal woven bone area, periosteal bone surface (BS), mineral apposition rate (MAR), mineralizing surface (MS/BS), and bone formation rate (BFR/BS), as per convention [30].

Immunohistochemistry

Histological analysis was performed at 3d and 7d after loading (20 rats total; n=4–5/group/time point). Forelimbs were dissected to include the intact radius and ulna with a small amount of surrounding muscle. These were fixed in 10% formalin at room temperature (RT), decalcified in 14% EDTA (RT, 2 weeks) and embedded in paraffin. Transverse sections were cut at the location of callus midpoint (5μm thickness). Several stains were performed on serial sections and imaged using NanoZoomer (Hamamatsu NanoZoomer HT model, 20x images). Hematoxylin and eosin (H&E) staining was performed on 3d and 7d sections. Von Willebrand factor (vWF), a protein produced by vascular endothelial cells and marker of angiogenesis [31, 32], was localized by immunohistochemistry at 3d and 7d [23].

Per the manufacturer's instructions (ABC Rabbit Kit, Santa Cruz) overnight antigen retrieval was performed with 0.33M boric acid at 55ºC, followed by overnight primary incubation (Millipore AB7356, 1:200). These sections were not counterstained. Each slide was numbered to allow blinded analysis under light field microscopy (TSS) in which number of vWF+ blood vessels was counted and normalized by the callus area (Bioquant). Proliferating Cell Nuclear Antigen (PCNA), expressed during DNA synthesis, was localized at 3d to examine cell proliferation. PCNA staining was performed following manufacturer's instruction (PCNA staining kit, Invitrogen), with sodium citrate antigen retrieval (10 min at 95ºC), 10min DAB, and counterstained with hematoxylin. PCNA positive cells, total cells, and callus area were quantified (JAM). Tartrate-resistant acid phosphatase (TRAP) staining was performed at 7d to evaluate fracture callus osteoclast activity. Deparaffinized sections were incubated with 0.2M acetate buffer for 20min at RT then incubated at 37 ºC adding 0.5 mg/ml naphthol AS-MX phosphate and 1.1 mg/ml fast red TR salt. Following rinsing sections were counterstained in Mayer's hematoxylin. TRAP positive cells and callus area were quantified (JAM).

Statistical Analysis

A priori power analysis was performed using historical coefficients of variance. To account for attrition, n=7 was chosen for qRT-PCR experiments, as n=6 is required to detect a 70% (1.7-fold) change in gene expression with a coefficient of variance of 43%, α error of 0.05, and β error of 0.2. For dynamic histomorphometric study of cortical bone, n=11 was chosen (n=10 required to detect a 37% change in bone area and 33% change in mineralizing surface, with a coefficient of variance of 32%, α error of 0.05, and β error of 0.2. A sample size of 9–10 was used for dynamic histomorphometric analysis of cancellous bone sections, and for immunohistochemistry analysis n=4–5 was used. Two-way ANOVA and Fischer least significant difference analysis were performed *post-hoc* to determine differences between vehicle (DMSO) and treatment (GDC-0449) groups, and to evaluate changes between time points. Paired student's t-test was used determine differences between RU (loaded) and LU (non-loaded). Unpaired student's t-test was employed to determine differences between experimental groups for assays with continuous variable data. P-values ≤ 0.05 constituted statistical significance.

Results

Drug Treatment

Administration of GDC-0449 was moderately well-tolerated. Weight declined over the course of the experiment in both vehicle and GDC-0449 groups. Weight loss was significantly less in vehicle rats used for dynamic histomorphometric and microCT analyses (versus GDC-0449 at 7d), although the absolute difference was small (−11.7 versus −15.1%, respectively; p=0.0007). There were no differences in weight loss between the vehicle and GDC-0449 rats used in qRT-PCR studies (−4 versus −5% at 1d, p=0.54; −9 versus −11% at 3d, p=0.16), nor for those used in immunohistochemistry studies (−8 versus −11% at 3d, p=0.24; −12.9 versus −12.7% at 7d, p=0.96). No vehicle rats died (100% survival). Three rats in the GDC-0449 group died (91% survival); two during mechanical loading (presumed anesthesia overdose), and one 2d after loading (cause unknown).

Hedgehog pathway was activated in response to stress fracture

To evaluate the natural course of Hh signaling changes in response to loading-induced stress fracture, expression of Ptch1, Gli1, Hhip, and Hh ligands was determined by qRT-PCR for vehicle animals. Expression of Ptch1 and Gli1 was upregulated at 3d within the RU callus, but not at 1d, in response to stress fracture (Figure 1A). From 1d to 3d, Ptch1 and Gli1 expression both increased significantly (1.7- and 1.8-fold, respectively).

In regard to Hh ligands, Shh expression was upregulated (1.8-fold) at 1d in response to loading, but not at 3d (Figure 1B). Ihh expression was upregulated at 3d but not at 1d, and no significant changes were observed over this time course. Dhh expression was upregulated at 1d (2.3-fold) and 3d (1.5-fold) after loading, however expression decreased by 50% between 1d and 3d.

GDC-0449 systemically inhibited hedgehog signaling and blocked the upregulation of hedgehog genes after stress fracture

GDC-0449 significantly reduced expression of the Hh target genes Gli1, Ptch1, and Hhip within the fracture callus of the right ulna (RU), as well as within the corresponding diaphyseal segment of the non-loaded left ulna (LU) as determined by qRT-PCR (Figure 1A, 1C). As early as 1d after stress fracture, GDC-0449 exerted a strong inhibitory effect, as Gli1, Ptch1, and Hhip expression was significantly reduced to 22–63% of vehicle expression levels in both the RU and LU (Figure 1C). Marked and significant inhibition of the Hh pathway was also observed at 3d, with expression of Gli1, Ptch1, and Hhip reduced to 6–50% of vehicle levels. The temporal upregulation of Ptch1 and Gli1 observed for the vehicle group between 1d and 3d was negated by GDC-0449 treatment, reducing Gli1 and Ptch1 expression at 3d by 47% and 46%, respectively (Figure 1A). Although Hhip expression did not increase between 1d and 3d in the vehicle group, its expression was significantly inhibited by GDC-0449 at both time points (46% reduction at 1d, 63% at 3d; Figure 1A).

Expression of Hh ligands (Shh, Ihh, Dhh) was evaluated at 1d and 3d to determine the effects of GDC-0449 treatment (Figure 1B). GDC-0449 reduced Shh expression by 37% at 3d ($p<0.05$ versus vehicle), but no effect was observed at 1d. GDC-0449 treatment resulted in a 44% increase in Ihh expression between 1d and 3d, although expression was no different than for vehicle at either time point. The increase in Dhh expression observed in response to loading in the vehicle group was unaffected by GDC-0449 treatment at 1d or 3d.

Hedgehog inhibition impaired the healing response to loading-induced stress fracture by inhibiting woven bone formation

Review of microCT images revealed that each specimen sustained a mid-diaphyseal ulnar stress fracture without propagation of a full fracture. Based upon analysis of microCT data, GDC-0449 treatment decreased the woven bone volume by 37% at 7d (4.2 vs 2.6 mm^3; $p=0.0001$) (Figure 2A). GDC-0449 also reduced the woven bone BMD at 7d (−17%; 367 vs 314 mg HA/cm^3; $p<0.0001$) (Figure 2B). GDC-0449 did not affect the TMD of the diaphyseal cortical bone at 7d (Figure 2C). No difference in longitudinal crack extent was observed after mechanical loading, indicating that similar levels of damage were created by

loading in the vehicle and GDC-0449 groups (1.65 mm vs 1.59 mm, respectively; p=0.51) (Figure 2D).

Dynamic histomorphometric analysis revealed that the 7d fracture callus was comprised predominantly of woven bone in both vehicle and GDC-0449 groups (Figure 2E), confirming that the callus visualized with microCT represented woven bone. Periosteal woven bone area was reduced by 29% by GDC-0449 at 7d (0.087 vs 0.062 mm^2; p=0.003; Figure 2F), paralleling the microCT finding of reduced woven bone volume.

Osteogenic gene expression increased in response to fracture, and was reduced by hedgehog inhibition

Expression of Alpl, Osx, and Ibsp was upregulated in the RU at 1d and 3d, indicating that mechanical loading induced osteogenic gene expression (Figure 3). Expression of Alpl, Osx, and Ibsp increased significantly between 1d and 3d in the RU from both the vehicle and GDC-0449 groups (Figure 3A). Over this time course, Alpl expression increased 2.9-fold in both groups. Osx expression increased by 2.5- and 2.9-fold in vehicle and GDC-0449 groups, respectively, and Ibsp expression increased 4.0- and 3.9-fold, respectively. GDC-0449 treatment significantly reduced expression of Alpl at 1d and 3d for both the left (−23% and −34%, respectively) and right ulnae (−24%, and −37%, respectively). GDC-0449 significantly reduced Ibsp expression only for the right ulna at 3d (−19%), and had no effect on Osx expression.

Chondrogenic gene expression was unaffected by hedgehog inhibition

Expression of Acan and Sox9 increased between 1d and 3d for both the vehicle and GDC-0449 groups. However, GDC-0449 treatment did not influence their expression at either time point (Supplemental Figure 1). GDC-0449 treatment led to a 28% increase in Sox9 expression at 3d, but this did not reach statistical significance (p=0.059). Col2α1 expression was significantly downregulated in the right (loaded) ulna in both groups at both time points, but was unaffected by GDC-0449 treatment.

Early cellular proliferation within the fracture callus was not influenced by hedgehog inhibition

Periosteal expansion in the region of the stress fracture was observed by routine histology, with less expansion in GDC-0449 treated ulnae than controls based on qualitative observation (Figure 4A). To evaluate cellular proliferation, PCNA immunohistochemistry was performed and the number and percentage of cells staining positively for PCNA were calculated. There was no difference observed between vehicle and GDC-0449 groups for the right ulna at 3d, either for PCNA-positive cell number (1030 vs. 998 #/mm^2, p = 0.94) or for percentage of positive cells (16.4 vs 15.5%, p=0.88; Figure 4B).

Bone resorption metrics were not increased by hedgehog inhibition

Left and right ulnae were subjected to TRAP staining followed by qualitative and quantitative assessment at 7d (Figure 5). The number of osteoclasts within the fracture callus involved in active bone resorption, as determined by TRAP staining, was dramatically reduced in the GDC-0449 group (47.2 vs 5.0; p=0.009). To determine whether hedgehog-

mediated alteration of Tnfsf11 (Rankl) or Tnfrsf11b (Opg) expression was responsible for this difference, qRT-PCR was employed. Although Rankl and Opg expression were upregulated in the right ulna in both groups at 1d and 3d, no differences were observed between vehicle and GDC-0449 groups. In contrast to the right ulna, GDC-0449 treatment did not affect the already low number of active osteoclasts in the corresponding mid-portion of the left (non-loaded) ulna.

Hedgehog signaling mediated the angiogenic response to stress fracture

In response to stress fracture, expression of Hif1α and Pecam1 was upregulated (Figure 6A). GDC-0449 decreased Hif1α expression by 30% at 3d. GDC-0449 did not influence the expression of Hif1α at 1d, or expression of Pecam1 at either time point. Figure 6B shows representative vWF immunohistochemistry photomicrographs of loaded mid-callus RU paraffin sections at 3d and 7d. GDC-0449 reduced blood vessel density by 55% at 3d, but had no effect at 7d.

Hedgehog inhibition impaired lamellar bone formation in both non-loaded and loaded cortical bone (ulna), but not in non-loaded cancellous bone (tibia)

In this model, 7d of treatment with GDC-0449 diminished periosteal lamellar bone formation. In the non-loaded ulna MAR was not significantly different ($p=0.056$), while BFR/BS was decreased by 37% ($p=0.003$) in GDC-0449 group vs. vehicle (Figure 7A). In lamellar sections from the loaded RU (cortical bone section adjacent to the proximal extent of the woven bone callus; Figure 7B), MAR was decreased by 17% ($p=0.006$) and BFR/BS reduced by 20% ($p=0.043$). In contrast, GDC-0449 treatment did not affect cancellous bone formation measured in the tibial metaphysis at 7d (MAR, $p=0.61$; BFR/BS, $p=0.71$; Figure 7C). Thus, periosteal lamellar bone formation was diminished by GDC-0449 treatment whereas cancellous bone formation was unaffected.

Discussion

The primary purpose of this study was to determine whether Hh signaling is a requirement for the osteogenic and angiogenic responses during stress fracture healing, while a secondary purpose was to determine whether Hh plays a role in post-natal bone homeostasis. We confirmed that Hh signaling is upregulated in response to mechanical loading-induced stress fracture in the adult rat. To validate our experimental model of Hh inhibition, we showed that systemic GDC-0449 treatment strongly reduced the expression of Hh target genes (Gli1, Ptch1, and Hhip) at 1d and 3d after stress fracture in both the loaded and non-loaded ulnae. In support of our hypothesis that the woven bone healing response to stress fracture is a Hh-dependent process, we demonstrated that Hh inhibition significantly reduced callus volume (−37%) and mineral density (−17%) at 7d. In support of our hypothesis that the angiogenic response to stress fracture is Hh-dependent, we showed that Hh inhibition significantly reduced blood vessel density within the healing callus at 3d after stress fracture, with concomitant upregulation of Hif1α indicative of relative local hypoxia. Finally, we showed that Hh inhibition significantly reduced the rate of cortical lamellar, but not cancellous, bone formation at 7d.

Our most significant finding is that new bone formation, both woven and cortical lamellar, is Hh dependent in the adult skeleton. To clarify the cellular basis responsible for this finding, further studies were performed to determine whether differences in osteogenic and chondrogenic gene expression, cellular proliferation, mineralization, or bone resoprtion may be responsible. We conclude that this decrease in woven bone observed in the presence of GDC-0449 treatment is unlikely to be mediated through alterations in early cellular proliferation, given our finding that the number and percentage of PCNA-positive cells within the stress fracture callus was unaffected by Hh inhibition at 3d. Changes in osteoblastic differentiation are also unlikely responsible, as early expression of the critical osteoblastic transcription factor Osx was unaffected by Hh inhibition. Given that the number of active osteoclasts was actually greater within the vehicle group callus at 7d (likely representative of a direct Hh effect on osteoclast differentiation[33]) and that Hh inhibition had no effect on the expression of Rankl and Opg at 1d and 3d, we conclude that elevated bone resorption is unlikely responsible for our observed Hh-mediated decrease in woven bone. We also evaluated chondrogenic gene expression within the callus, in part because diminished bone formation or woven bone density may have been due to a shift toward endochondral bone formation. However, Hh inhibition did not influence the expression of Acan, Sox9, or Col2α1 at 1d or 3d after fracture. Therefore, we conclude that the observed difference in woven bone mineral density is not due to changes in chondrogenic gene expression at the time points examined. Furthermore, all loaded 7d dynamic histomorphometry sections revealed strong calcein and alizarin labeling for both vehicle and GDC-0449 groups, suggesting no effect on mineralization per se. In contrast, the decrease in woven bone volume in rats treated with the Hh pathway inhibitor paralleled our observed decrease in Alpl expression at 1d and 3d, and the decrease in Ibsp expression at 3d. Combined, we conclude that a reduction in bone formation was the responsible mechanism underlying the observed Hh-mediated decrease in woven bone.

A robust, periosteal vascular response is known to occur after stress fracture [23, 29]. Here we observed that the early (3d) increase in vessel density was blunted by GDC-0449 treatment. Combined with our observed concomitant decrease in early osteogenic gene expression, we are unable to conclude whether the decrease in blood vessel density seen with Hh inhibition is a primary effect, or secondary to a decrease in osteogenesis. However, it is clear that the decrease in callus vessel density occurred independently of Pecam1 expression, which was unaffected by Hh inhibition. Hh inhibition resulted in a higher level of Hif1α expression at 3d (30%), which may indicate relative avascularity and hypoperfusion within the healing callus. Combined, a decrease in early callus vessel density with increased signs of local tissue hypoxia favor a primary effect of the Hh pathway in regulating angiogenesis during stress fracture healing. There were no differences in blood vessel density observed at 7d, suggesting that the Hh pathway exerts its angiogenic effects early in the process of fracture healing – this is consistent with findings reported by several groups [34–37]. Bijlsma *et al* showed that hypoxia was capable of triggering Hif1α-mediated hedgehog pathway activation [36]. Systemic upregulation of Shh and Ptch1 expression was observed after as little as 4h in mice subjected to normobaric hypoxia - this effect was also specifically noted in fibroblasts and cardiomyocytes, and was prevented by Hif1α knockdown [36]. A study by Renault *et al* further supports the importance of the Hh

pathway as a regulator of angiogenesis. Using a murine corneal angiogenesis model, Shh enhanced endothelial cell migration and increased capillary morphogenesis in a Matrigel culture system [37]. Although previous studies have implicated the hedgehog pathway as an important regulator of VEGF signaling and the production of angiopoietins[34, 35, 38, 39], further investigation is indicated to determine the mechanism responsible for our observation that Hh inhibition impairs angiogenesis during early stress fracture healing.

Our results demonstrate that normal post-natal cortical bone formation is Hh-dependent, as GDC-0449 reduced periosteal lamellar bone formation in both loaded and non-loaded ulnae. Interestingly, cancellous bone formation in non-loaded tibiae was not influenced by Hh inhibition. Thus, Hh signaling may be critical for periosteal lamellar bone formation as part of post-natal bone modeling, but not for cancellous bone formation as part of bone remodeling. The underlying mechanism responsible for these disparate effects is unclear, although we acknowledge that our evaluation of the tibial cancellous site was limited, and it is premature to make any conclusions about the role of Hh in post-natal cancellous bone. Nonetheless, the observed effects on cortical bone indicate that the Hh pathway influences bone formation under basal conditions, in addition to its influence on woven bone formation and angiogenesis during stress fracture healing.

This study has several additional limitations. The study time frame did not extend beyond 7 days, so it is unclear if Hh inhibition results in a delay in healing versus prevention of complete healing. Furthermore, biomechanical properties of the healing stress fracture callus were not evaluated. The woven bone healing response observed for this rat stress fracture model is characterized by non-endochondral ossification [27], which differs from full fracture healing that involves non-endochondral and endochondral ossification [40]. Although stress fractures are clinically relevant, insight into whether Hh regulates full fracture healing is also of interest. A recent finding indicated that osteoblast-specific blockade of Smo markedly decreased fracture callus volume in stabilized murine tibial mid-diaphyseal complete fractures, whereas chondrocyte-specific blockade had no effect. [26] With our findings, these results indicate a critical role for Hh signaling in the non-endochondral stages of bone repair.

In summary, we demonstrated that Hh signaling is critical for woven bone formation in the healing response to stress fracture. The underlying mechanism by which the Hh pathway modulates woven bone formation in this setting involves direct impairment of bone formation, as in our experimental model Hh inhibition did not affect cellular proliferation, chondrogenic gene expression, Osx expression, or metrics of bone resoprtion within the periosteal fracture callus. Furthermore, the Hh pathway promotes angiogenesis early in this setting, as its blockade decreases the amount of vessels that form and leads to increased Hif1α expression suggestive of relative tissue hypoxia. The Hh pathway also plays a role in post-natal bone modeling, as its inhibition decreases lamellar bone formation rate in both the loaded and non-loaded ulnae (cortical bone). These findings support an important role for Hh signaling in the post-natal skeleton.

Supplementary Material

Refer to Web version on PubMed Central for supplementary material.

Acknowledgments

NIH/NIAMS R01 AR050211 (MJS). NIH P30 AR057235 (MJS - Washington University Musculoskeletal Research Center). Orthopaedic Research and Education Foundation (OREF) Resident Scientist Training Grant (NHK). NIH/NIDDK R01 DK065789 (FL). NCRR 1S10RR027552 (Nanozoomer Shared Instrumentation Grant).

Non-Standard Abbreviations

Hh	Hedgehog
LU	Left ulna
RT	Room temperature
RU	Right ulna

References

1. Ingham PW, McMahon AP. Hedgehog signaling in animal development: paradigms and principles. Genes Dev. 2001; 15(23):3059–87. [PubMed: 11731473]
2. McMahon AP, Ingham PW, Tabin CJ. Developmental roles and clinical significance of hedgehog signaling. Curr Top Dev Biol. 2003; 53:1–114. [PubMed: 12509125]
3. Day TF, Yang Y. Wnt and hedgehog signaling pathways in bone development. J Bone Joint Surg Am. 2008; 90 (Suppl 1):19–24. [PubMed: 18292352]
4. Dai P, Akimaru H, Tanaka Y, Maekawa T, Nakafuku M, Ishii S. Sonic Hedgehog-induced activation of the Gli1 promoter is mediated by GLI3. J Biol Chem. 1999; 274(12):8143–52. [PubMed: 10075717]
5. Vokes SA, Ji H, McCuine S, Tenzen T, Giles S, Zhong S, et al. Genomic characterization of Gli-activator targets in sonic hedgehog-mediated neural patterning. Development. 2007; 134(10):1977–89. [PubMed: 17442700]
6. Chuang PT, McMahon AP. Vertebrate Hedgehog signalling modulated by induction of a Hedgehog-binding protein. Nature. 1999; 397(6720):617–21. [PubMed: 10050855]
7. Agren M, Kogerman P, Kleman MI, Wessling M, Toftgard R. Expression of the PTCH1 tumor suppressor gene is regulated by alternative promoters and a single functional Gli-binding site. Gene. 2004; 330:101–14. [PubMed: 15087129]
8. Chen JK, Taipale J, Cooper MK, Beachy PA. Inhibition of Hedgehog signaling by direct binding of cyclopamine to Smoothened. Genes Dev. 2002; 16(21):2743–8. [PubMed: 12414725]
9. Robarge KD, Brunton SA, Castanedo GM, Cui Y, Dina MS, Goldsmith R, et al. GDC-0449-a potent inhibitor of the hedgehog pathway. Bioorg Med Chem Lett. 2009; 19(19):5576–81. [PubMed: 19716296]
10. Rudin CM, Hann CL, Laterra J, Yauch RL, Callahan CA, Fu L, et al. Treatment of medulloblastoma with hedgehog pathway inhibitor GDC-0449. N Engl J Med. 2009; 361(12): 1173–8. [PubMed: 19726761]
11. Yue Q, Chen YH, Mulder T, Deese A, Takahashi R, Rudewicz PJ, et al. Absorption, distribution, metabolism, and excretion of [(1)C]GDC-0449 (vismodegib), an orally active hedgehog pathway inhibitor, in rats and dogs: a unique metabolic pathway via pyridine ring opening. Drug Metab Dispos. 2011; 39(6):952–65. [PubMed: 21363998]
12. LoRusso PM, Rudin CM, Reddy JC, Tibes R, Weiss GJ, Borad MJ, et al. Phase I trial of hedgehog pathway inhibitor vismodegib (GDC-0449) in patients with refractory, locally advanced or metastatic solid tumors. Clin Cancer Res. 2011; 17(8):2502–11. [PubMed: 21300762]

13. Amin SH, Tibes R, Kim JE, Hybarger CP. Hedgehog antagonist GDC-0449 is effective in the treatment of advanced basal cell carcinoma. Laryngoscope. 2010; 120(12):2456–9. [PubMed: 20927781]
14. Ehlen HW, Buelens LA, Vortkamp A. Hedgehog signaling in skeletal development. Birth Defects Res C Embryo Today. 2006; 78(3):267–79. [PubMed: 17061262]
15. Chiang C, Litingtung Y, Lee E, Young KE, Corden JL, Westphal H, et al. Cyclopia and defective axial patterning in mice lacking Sonic hedgehog gene function. Nature. 1996; 383(6599):407–13. [PubMed: 8837770]
16. Riddle RD, Johnson RL, Laufer E, Tabin C. Sonic hedgehog mediates the polarizing activity of the ZPA. Cell. 1993; 75(7):1401–16. [PubMed: 8269518]
17. Pagan SM, Ros MA, Tabin C, Fallon JF. Surgical removal of limb bud Sonic hedgehog results in posterior skeletal defects. Dev Biol. 1996; 180(1):35–40. [PubMed: 8948572]
18. Hojo H, Ohba S, Yano F, Saito T, Ikeda T, Nakajima K, et al. Gli1 protein participates in Hedgehog-mediated specification of osteoblast lineage during endochondral ossification. J Biol Chem. 2012; 287(21):17860–9. [PubMed: 22493482]
19. Long F, Chung UI, Ohba S, McMahon J, Kronenberg HM, McMahon AP. Ihh signaling is directly required for the osteoblast lineage in the endochondral skeleton. Development. 2004; 131(6): 1309–18. [PubMed: 14973297]
20. Hu H, Hilton MJ, Tu X, Yu K, Ornitz DM, Long F. Sequential roles of Hedgehog and Wnt signaling in osteoblast development. Development. 2005; 132(1):49–60. [PubMed: 15576404]
21. St-Jacques B, Hammerschmidt M, McMahon AP. Indian hedgehog signaling regulates proliferation and differentiation of chondrocytes and is essential for bone formation. Genes Dev. 1999; 13(16):2072–86. [PubMed: 10465785]
22. Ito H, Akiyama H, Shigeno C, Iyama K, Matsuoka H, Nakamura T. Hedgehog signaling molecules in bone marrow cells at the initial stage of fracture repair. Biochem Biophys Res Commun. 1999; 262(2):443–51. [PubMed: 10462495]
23. McKenzie JA, Silva MJ. Comparing histological, vascular and molecular responses associated with woven and lamellar bone formation induced by mechanical loading in the rat ulna. Bone. 2011; 48(2):250–8. [PubMed: 20849995]
24. Le AX, Miclau T, Hu D, Helms JA. Molecular aspects of healing in stabilized and non-stabilized fractures. J Orthop Res. 2001; 19(1):78–84. [PubMed: 11332624]
25. Murakami S, Noda M. Expression of Indian hedgehog during fracture healing in adult rat femora. Calcif Tissue Int. 2000; 66(4):272–6. [PubMed: 10742444]
26. Baht GS, Silkstone D, Nadesan P, Whetstone H, Alman BA. Activation of hedgehog signaling during fracture repair enhances osteoblastic-dependent matrix formation. J Orthop Res. 2014; 32(4):581–6. [PubMed: 24347536]
27. Uthgenannt BA, Kramer MH, Hwu JA, Wopenka B, Silva MJ. Skeletal self-repair: stress fracture healing by rapid formation and densification of woven bone. J Bone Miner Res. 2007; 22(10): 1548–56. [PubMed: 17576168]
28. Uthgenannt BA, Silva MJ. Use of the rat forelimb compression model to create discrete levels of bone damage in vivo. J Biomech. 2007; 40(2):317–24. [PubMed: 16519891]
29. Wohl GR, Towler DA, Silva MJ. Stress fracture healing: fatigue loading of the rat ulna induces upregulation in expression of osteogenic and angiogenic genes that mimic the intramembranous portion of fracture repair. Bone. 2009; 44(2):320–30. [PubMed: 18950737]
30. Dempster DW, Compston JE, Drezner MK, Glorieux FH, Kanis JA, Malluche H, et al. Standardized nomenclature, symbols, and units for bone histomorphometry: a 2012 update of the report of the ASBMR Histomorphometry Nomenclature Committee. J Bone Miner Res. 2013; 28(1):2–17. [PubMed: 23197339]
31. Schmeisser A, Garlichs CD, Zhang H, Eskafi S, Graffy C, Ludwig J, et al. Monocytes coexpress endothelial and macrophagocytic lineage markers and form cord-like structures in Matrigel under angiogenic conditions. Cardiovasc Res. 2001; 49(3):671–80. [PubMed: 11166280]
32. Zanetta L, Marcus SG, Vasile J, Dobryansky M, Cohen H, Eng K, et al. Expression of Von Willebrand factor, an endothelial cell marker, is up-regulated by angiogenesis factors: a potential

method for objective assessment of tumor angiogenesis. Int J Cancer. 2000; 85(2):281–8. [PubMed: 10629090]

33. Heller E, Hurchla MA, Xiang J, Su X, Chen S, Schneider J, et al. Hedgehog signaling inhibition blocks growth of resistant tumors through effects on tumor microenvironment. Cancer Res. 2012; 72(4):897–907. [PubMed: 22186138]
34. Dohle E, Fuchs S, Kolbe M, Hofmann A, Schmidt H, Kirkpatrick CJ. Comparative study assessing effects of sonic hedgehog and VEGF in a human co-culture model for bone vascularisation strategies. Eur Cell Mater. 2011; 21:144–56. [PubMed: 21305477]
35. Dohle E, Fuchs S, Kolbe M, Hofmann A, Schmidt H, Kirkpatrick CJ. Sonic hedgehog promotes angiogenesis and osteogenesis in a coculture system consisting of primary osteoblasts and outgrowth endothelial cells. Tissue Eng Part A. 2010; 16(4):1235–7. [PubMed: 19886747]
36. Bijlsma MF, Groot AP, Oduro JP, Franken RJ, Schoenmakers SH, Peppelenbosch MP, et al. Hypoxia induces a hedgehog response mediated by HIF-1alpha. J Cell Mol Med. 2009; 13(8B): 2053–60. [PubMed: 18774959]
37. Renault MA, Roncalli J, Tongers J, Thorne T, Klyachko E, Misener S, et al. Sonic hedgehog induces angiogenesis via Rho kinase-dependent signaling in endothelial cells. J Mol Cell Cardiol. 2010; 49(3):490–8. [PubMed: 20478312]
38. Moran CM, Myers CT, Lewis CM, Krieg PA. Hedgehog regulates angiogenesis of intersegmental vessels through the VEGF signaling pathway. Dev Dyn. 2012; 241(6):1034–42. [PubMed: 22513894]
39. Chen W, Tang T, Eastham-Anderson J, Dunlap D, Alicke B, Nannini M, et al. Canonical hedgehog signaling augments tumor angiogenesis by induction of VEGF-A in stromal perivascular cells. Proc Natl Acad Sci U S A. 2011; 108(23):9589–94. [PubMed: 21597001]
40. Einhorn TA. The cell and molecular biology of fracture healing. Clin Orthop Relat Res. 1998; 355(Suppl):S7–21. [PubMed: 9917622]

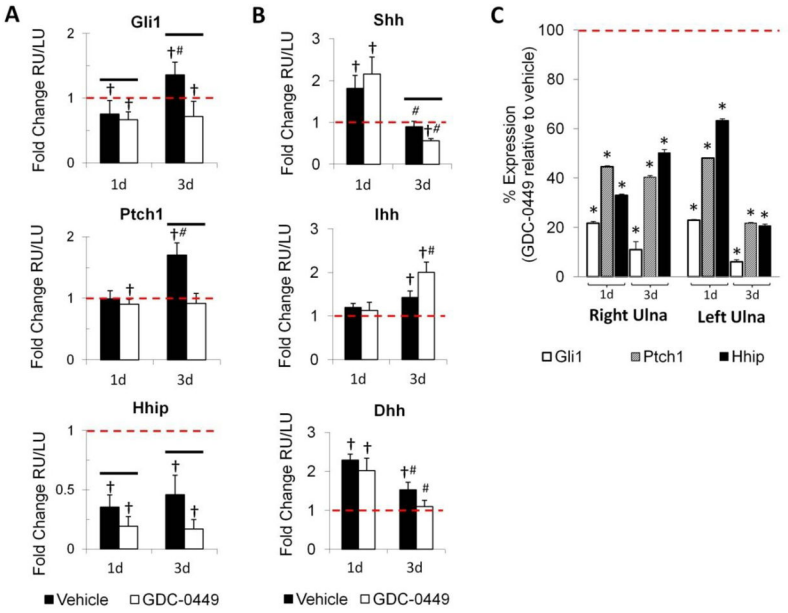

Figure 1.

Gene expression analysis demonstrated that the Hedgehog pathway was activated in response to stress fracture, and was systemically inhibited by GDC-0449 in the adult rat experimental model. **(A)** Loading induced the upregulation of Hh pathway mediators Gli1 and Ptch1 at 3d; an effect that was attenuated by GDC-0449. Hhip expression was suppressed after loading. **(B)** Loading induced the upregulation of Shh and Dhh at 1d and Ihh at 3d; these responses were not diminished by GDC-0449 treatment. **(C)** GDC-0449 treatment systemically reduced expression of hedgehog pathway mediators Gli1, Ptch1 and Hhip in both the loaded right ulna and non-loaded left ulna. Represented is the percent reduction in gene expression as a result of GDC-0449 treatment, as compared to vehicle ($2^{-\Delta Cq}$ GDC-0449/$2^{-\Delta Cq}$ vehicle * 100%, where 100% represents vehicle expression level). Data represents mean ± SEM. *$p<0.05$ vehicle vs GDC-0449, $^{\#}p<0.05$ 1d vs 3d, †$p<0.05$ RU vs LU. n=6–7 for gene expression data.

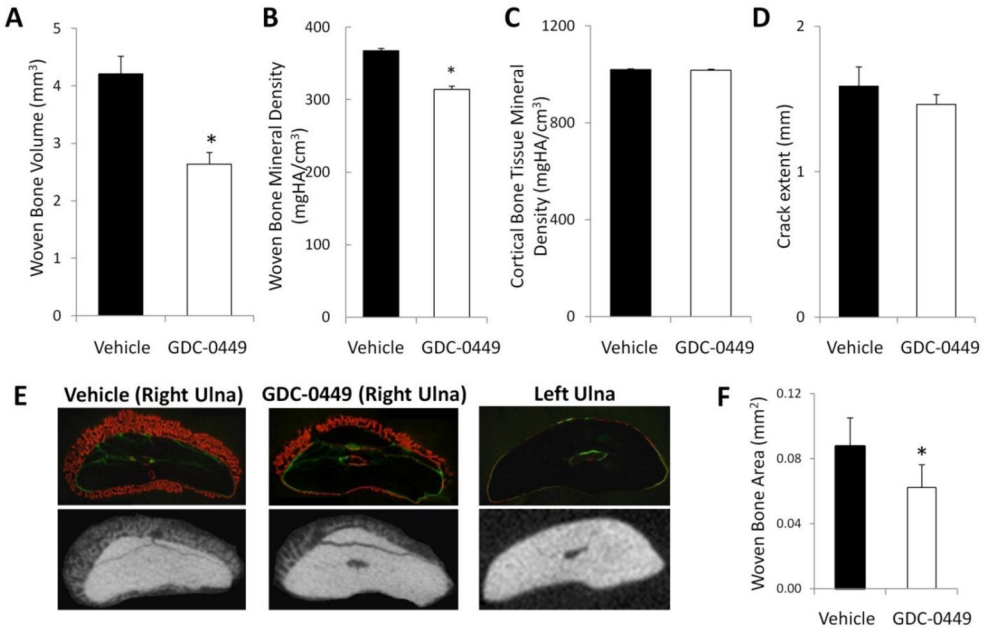

Figure 2.

Hh inhibition impairs the healing response to loading-induced stress fracture by inhibiting woven bone formation and decreasing mineral content. **(A)** GDC-0449 decreased woven bone volume by 37% (p=0.0001) and **(B)** decreased woven bone BMD by 17% (p<0.0001). **(C)** GDC-0449 did not affect cortical TMD after 7d of treatment (*p*=0.84). (**D)** Analysis of the longitudinal crack extent revealed that forelimb loading produced similar levels of damage between vehicle and GDC-0449 groups (p=0.51). **(E)** Represented are dynamic histomorphometric and microCT images at 7d from the axial midpoint of the callus for the loaded right ulna (RU) for vehicle and GDC-0449 groups, and from the corresponding segment of non-loaded left ulna (LU). Dynamic histomorphometry revealed that at 7d, the callus was comprised predominantly of woven bone in both the vehicle and GDC-0449 groups. The non-loaded LU did not contain any woven bone. **(F)** GDC-0449 significantly decreased periosteal woven bone area by 29% at 7d, as determined by dynamic histomorphometric analysis of the fracture callus axial midpoint section (p=0.003). Data represents mean ± SEM. *p<0.05 vehicle vs GDC-0449. n=13–14 for microCT data, n=9–10 for dynamic histomorphometry.

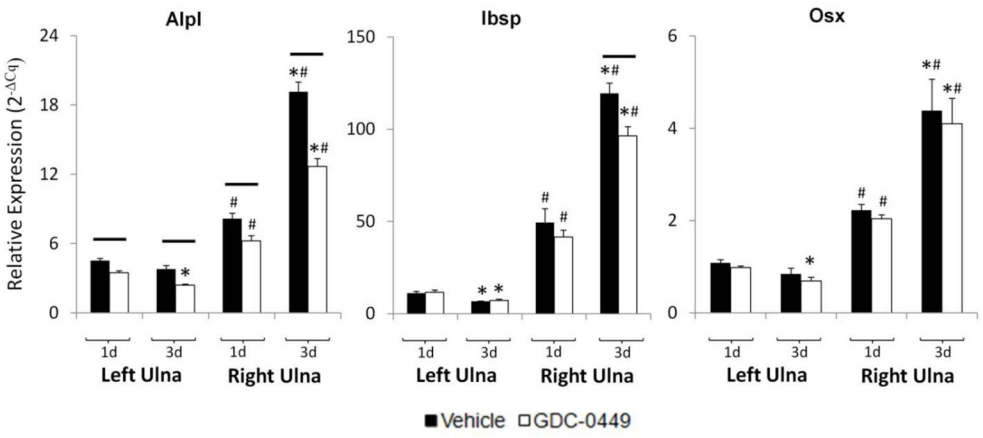

Figure 3.

Osteogenic gene expression increased in response to fracture, and was reduced by GDC-0449. Expression of select osteogenic markers Alpl, Ibsp, Osx within the fracture callus increased significantly between 1d and 3d after loading in both the vehicle and GDC-0449 groups. Alpl expression was significantly reduced by GDC-0449 in both the left (non-loaded) and right (loaded) ulnae at 1d and 3d. GDC-0449 treatment reduced expression of Ibsp in the right ulna at 3d, but no differences were observed at 1d or in the left ulna at either time point. Expression of Osx, a master regulatory transcription factor for osteoblastic differentiation, was unaffected by GDC-0449 treatment for both ulnae at 1d and 3d. Data represents mean ± SEM. *$p<0.05$ 1d vs 3d, $^{\#}p<0.05$ left ulna (LU) vs right ulna (RU), solid bar $p<0.05$ vehicle vs GDC-0449. n=6–7 for gene expression data.

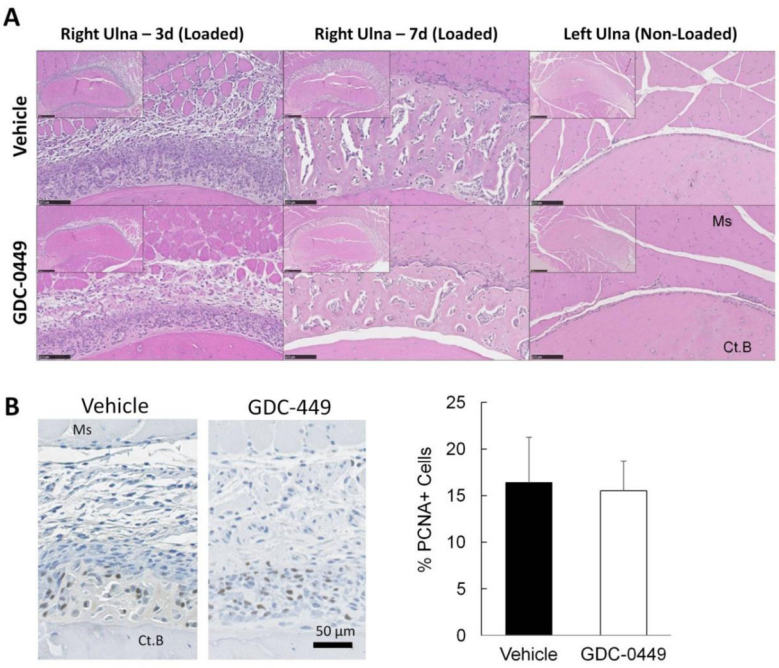

Figure 4.

Early cellular proliferation within the fracture callus was not influenced by GDC-0449. **(A)** Depicted are representative mid-callus sections after H&E staining imaged at low (5x) and high (20x) power. Qualitatively, the right ulna periosteal callus is less robust in the GDC-0449 group than the vehicle group at 3d and 7d. The non-loaded left ulna, which lacks callus, is included for comparison. Ms = muscle, CtB = cortical bone. Bars = 100μm. **(B)** Representative PCNA stained images depict most PCNA positive cells near the cortical surface for both the vehicle and GDC-0449. Quantitatively, the percentage of cells within the callus with positive PCNA staining was similar between groups at 3d. Bars = 50μm. Data represents mean ± SEM. n=4.

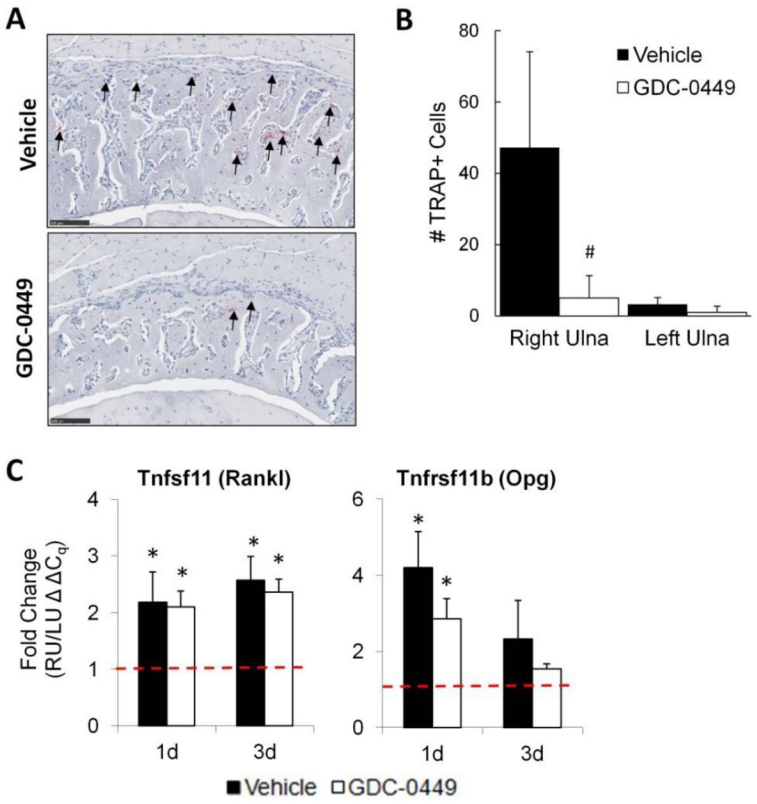

Figure 5.

Bone resorption metrics were not decreased by hedgehog inhibition. **(A)** Depicted are representative micrographs following TRAP staining at 7d. Qualitatively, many more TRAP-positive cells were observed in the vehicle group. Bars = 100μm. **(B)** The number of TRAP-positive cells within the right ulna callus at 7d was 90% less in the GDC-0449 group, as compared to the vehicle group. No difference was observed between vehicle and GDC-0449 groups for the left ulna at 7d. Results were unchanged when re-analyzed after normalizing for periosteal callus area (data not shown). **(C)** Tnfsf11 (Rankl) and Tnfrsf11b (Opg) expression was upregulated within the fracture callus of the right ulna at 1d and 3d, but was unaffected by GDC-0449. Data represents mean ± SEM. $^{\#}p<0.05$ vehicle vs GDC-0449, *$p<0.05$ RU vs LU. n=5 for TRAP data, n=7 for gene expression data.

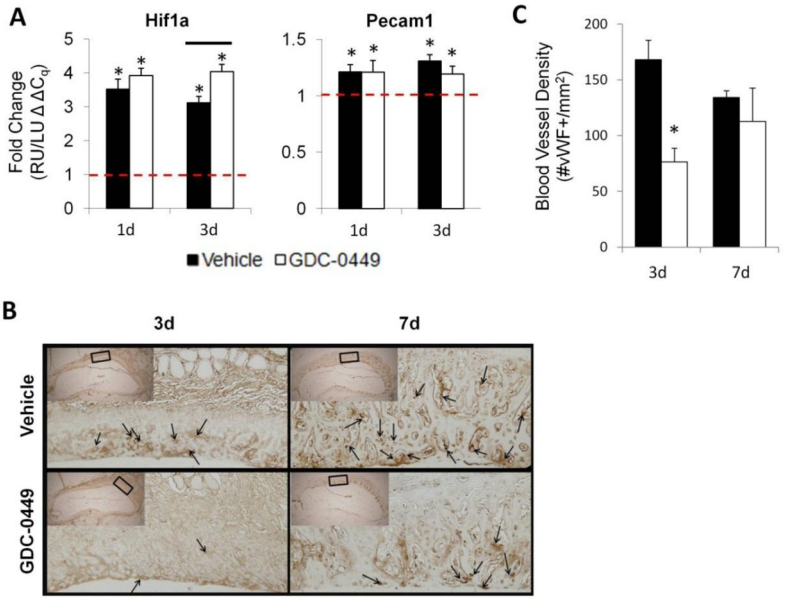

Figure 6.

Hedgehog signaling mediated the angiogenic response to stress fracture. **(A)** A 30% increase in Hif1α expression was observed with GDC-0449 treatment at 3d, as compared to vehicle. GDC-0449 did not otherwise influence the expression of Hif1α or Pecam1 at 1d or 3d. **(B)** Pictured are representative vonWillebrand factor (vWF) immunohistochemistry photomicrographs of loaded mid-callus right ulna (RU) paraffin sections at 3d and 7d. **(C)** Mid-callus blood vessel density (# vWF+/mm^2) was individually calculated for each rat by normalizing the number vessels with positive vWF staining by the periosteal woven bone area. GDC-0449 treatment resulted in a 55% reduction in blood vessel density at 3d (168 vs 76 vessels/μm^2; p=0.006), but no difference was observed at 7d (134 vs 113 vessels/μm^2; p=0.520). Data represents mean ± SEM. *p<0.05 right ulna (RU) vs left ulna (LU), bars p<0.05 vehicle vs GDC-0449. n=7 for gene expression data, n=4–5 for immunohistochemistry data.

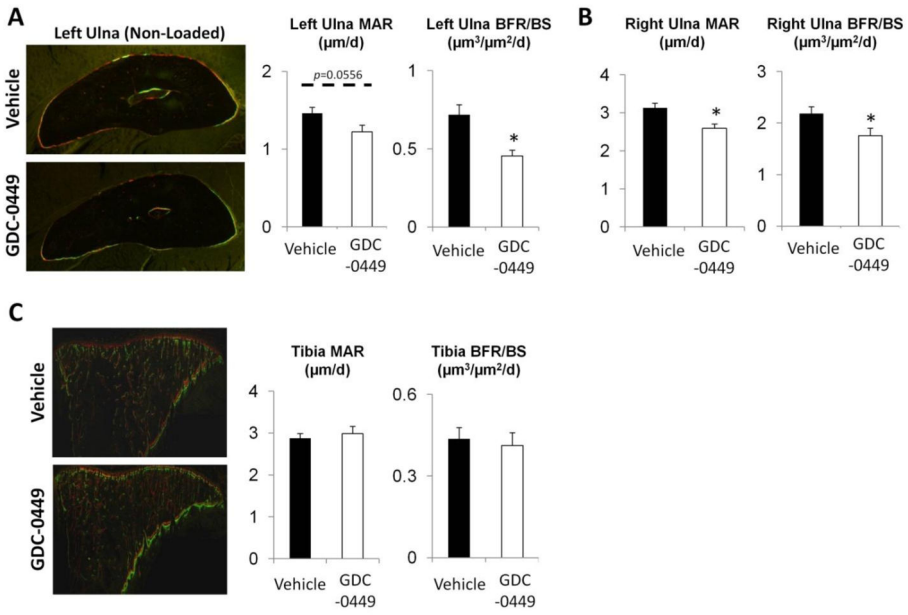

Figure 7.

Hh inhibition impaired periosteal lamellar bone but not cancellous bone formation. **(A)** GDC-0449 reduced mineral apposition rate (MAR) in non-loaded left ulna (LU) mid-diaphyseal cortical sections (1.46 vs 1.22 μm/d; p=0.056), and significantly decreased periosteal surface lamellar bone formation rate (BFR/BS) by 37% at 7d (0.72 vs 0.46 $\mu m^3/\mu m^2/d$; p=0.003). **(B)** Lamellar bone metrics were also decreased by GDC-0449 in loaded right ulnae (RU), as determined by dynamic histomorphometric analysis of cortical bone sections taken adjacent to the proximal end of the woven bone callus: MAR was reduced by 17% (3.13 vs 2.60 μm/d; p=0.006), and BFR/BS was reduced by 20% (2.19 vs 1.76 $\mu m^3/\mu m^2/d$; p=0.043). **(C)** Dynamic histomorphometric analysis of cancellous bone was also performed, with representative non-loaded tibial longitudinal sections pictured. GDC-0449 did not affect MAR (2.88 vs 2.99 μm/d; p=0.610) or BFR/BS (0.44 vs 0.41 $\mu m^3/\mu m^2/d$; p=0.709). Data represents mean ± SEM. *p<0.05 vehicle vs GDC-0449, dotted bar p<0.10 vehicle vs GDC-0449. n=9–10.